Morphological and Optical Characterization of Polyelectrolyte Multilayers Incorporating Nanocrystalline Cellulose

Emily D. Cranston and Derek G. Gray*

Department of Chemistry, Pulp and Paper Research Centre, McGill University, Montréal, Québec, H3A 2A7 Canada

Received March 24, 2006; Revised Manuscript Received July 3, 2006

Aqueous layer-by-layer (LbL) processing was used to create polyelectrolyte multilayer (PEM) nanocomposites containing cellulose nanocrystals and poly(allylamine hydrochloride). Solution-dipping and spin-coating assembly methods gave smooth, stable, thin films. Morphology was studied by atomic force microscopy (AFM) and scanning electron microscopy (SEM), and film growth was characterized by X-ray photoelectron spectroscopy (XPS), ellipsometry, and optical reflectometry. Relatively few deposition cycles were needed to give full surface coverage, with film thicknesses ranging from 10 to 500 nm. Films prepared by spin-coating were substantially thicker than solution-dipped films and displayed radial orientation of the rod-shaped cellulose nanocrystals. The relationship between film color and thickness is discussed according to the principles of thin film interference and indicates that the iridescent properties of the films can be easily tailored in this system.

Introduction

Today's knowledge of polymer and material science is due in no small part to the study of cellulose and its derivatives. Cellulose is the most abundant material in the biosphere, a long-chain polysaccharide composed of β-1,4-linked D-glucose rings. Microfibrils of crystalline cellulose form the primary structural component in plant cell walls, where superior mechanical properties result from strong hydrogen bonding and van der Waals forces between cellulose chains in crystallized hierarchical structures. By similar reasoning, cellulose does not dissolve in common solvents, and the discovery that cellulose can be acid-hydrolyzed to produce an aqueous suspension of nanocrystals[1,2] has substantially furthered its use in a vast range of materials. As a relatively cheap and accessible polymer, its useful characteristics include biodegradability, biocompatibility, nontoxicity, dimensional stability, high tensile strength, light weight, durability, and high hygroscopicity. Recently, much interest has been generated in replacing synthetic films, fibers, and composites with natural sources, and cellulose offers great promise in this respect.[3]

Past work on model cellulose surfaces[4−9] has most often used regenerated cellulose prepared from cellulose derivatives, due to the inherent difficulties in working with cellulose solvents. Ultrathin films of (carboxymethyl)cellulose and cellulose sulfate have also been designed and discussed in the literature for cell culture studies[10] and to investigate polymer adsorption.[11] Here we work with a stable aqueous colloidal suspension of cellulose in the native "cellulose I" crystal form, continuing the studies on model cellulose surfaces developed in our lab.[4] The nanocrystals in suspension are stabilized by negative surface charges (carboxyl or sulfate ester groups), which result from the hydrolysis process and give them certain polyelectrolyte properties.[12]

Electrostatic layer-by-layer (LbL) self-assembled films have been exploited for the fabrication of sophisticated nanocomposite materials.[13] In this method, a charged solid substrate is exposed to a solution of oppositely charged polyelectrolyte, followed by rinsing. The polymeric material adhering to the surface has more than the stoichiometric number of charges required for charge neutralization, thereby reversing the surface charge. This allows for easy adsorption of the next oppositely charged polyelectrolyte, also resulting in charge reversal. The amount of adsorbed polymer is self-limiting as a result of rinsing and allows for stepwise film growth. While generally performed with linear polyions, the procedure is suitable for a large range of multiple-charged nano-objects.[14] In this study, we show that nanocrystalline cellulose is amenable to sequential film growth by LbL assembly, as presented schematically in Figure 1.

The demand for films and coatings with tunable internal multilayered organization has led to much research in the field.[10,14−21] Structured LbL films have potential applications as antireflective coatings,[15] waveguides,[16,22] bio/optical sensors,[13,18] separation technologies,[13] drug delivery systems,[23,24] and electronic and photonic dielectric mirrors,[23] many of which are constructive steps toward fully functional molecular machines. These materials have also been used for micropatterning[25] and as nanogrowth templates[26] as yet another way to achieve desired macroscopic properties from nanoscopic ordering. Electrostatic multilayering is a versatile yet simple method that is well suited for automation with no inherent restrictions on polyelectrolyte type or substrate geometry. Adsorption kinetics and film properties can be tailored by changing the solution pH, ionic strength, polyelectrolyte molar mass and concentration, temperature, stirring/shear forces, and deposition time. Weak polyelectrolyte systems are more versatile than strong systems because the layer structure and swelling properties can be more accurately controlled by solution pH and salt concentration. Resultant films and coatings show long-life stability as well as self-healing characteristics.[18,27] Previous work has incorporated the linear polymer cellulose sulfate into polyelectrolyte multilayer films,[19,28] whereas here we describe the incorporation of colloidal cellulose nanocrystals.

Precise spatial control is required to develop materials with enhanced mechanical, optical, electrical, and permeation proper-

* To whom correspondence should be addressed: e-mail derek.gray@mcgill.ca; tel 514-398-6182.

10.1021/bm0602886 CCC: $33.50
Published on Web 08/18/2006

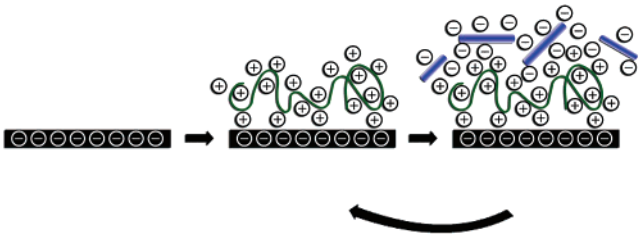

Figure 1. Schematic representation of the build-up of electrostatically adsorbed multilayered films. The polyelectrolyte, PAH, is shown by the curved line and colloidal cellulose nanocrystals are represented by straight rods; counterions have been omitted for clarity.

ties. Many attempts to incorporate colloids into LbL films have been successful.[14] Particularly, high-aspect-ratio charged colloids, similar to cellulose nanocrystals, have promising reinforcement capabilities and have included clay platelets,[21] inorganic sheets,[29] the tobacco mosaic virus,[30] and rod-shaped dye particles.[31] The aspect ratio of cellulose nanocrystals can be varied from 1:1 to 1:100 depending on the cellulose source and hydrolysis conditions, offering tailorable mechanical properties.[32,33] This has led to fabrication of nanocomposites containing cellulose nanocrystals in a variety of polymer matrices for applications ranging from transportation paneling to low thickness polymer electrolytes for lithium batteries.[3,34−39] Rigid anisotropic biomacromolecules such as DNA and proteins have also been used in LbL films designed for applications in drug delivery and gene therapy but are smaller than cellulose nanocrystals and do not enhance mechanical properties. The potential exists to create 3D photonic crystals,[20,40] optical sensors,[15] and tunable dielectric mirrors[16,23] from mulilayered colloidal particles, based on the principles of thin film interference and Bragg scattering. In this paper, we present the in-depth experimental results of incorporating organic, biocompatible, and bioinert needlelike cellulose particles into polyelectrolyte multilayer films, expanding on recent proof-of-principle work.[41,42] Poly(allylamine hydrochloride) was chosen for use as the polycation because it is well-known in LbL systems.[43] This study compares two of the most facile, economical, and efficient methods for LbL assembly of thin films: solution-dipping and spin-coating.

Conventionally, LbL assembly has employed solution-dipping (or dip-coating) in beakers of various sizes containing dilute aqueous polymer solutions. This inexpensive method works for most substrates independent of shape but has not always resulted in adequately homogeneous films. Alternatively, spin-coating is the most widely used technique for obtaining uniform films in lithography and other micromachining applications. The spin-coating process involves the acceleration of a liquid solution on a rotating substrate and is characterized by a balance of centrifugal forces (spin speed) and viscous forces (solution viscosity). Films created this way have been found to be consistent and reproducible in thickness,[44] showing enhanced local planarity when compared to solution-dipped films.[45] This procedure eliminates edge defects often seen in solution-dipped films, whereby surface tension draws the solvent over the lip of the substrate and removes excess fluid. Spin-coating has the advantage of requiring only small amounts of liquid to coat large areas. Relatively new in the multilayer field, spin-assembled LbL films are believed to be held together by both substantial entanglement between layers and electrostatic cross-linking. Spin-coating is mechanically controlled rather than thermodynamically controlled, giving novel film configurations that have recently gained attention.[44] These films are substantially different from merely spin-coating polyelectrolytes on a surface. The primary advantage of spin-coating, over solution-dipping, in LbL assembly is the ability to vary parameters such as concentration, viscosity, solvent type, and spin speed, leading to films with variable thickness, density, and roughness.[46]

In this paper, we use atomic force microscopy (AFM) and scanning electron microscopy (SEM) to investigate the surface morphology and film roughness of polyelectrolyte multilayers containing cellulose nanocrystals prepared by LbL assembly. X-ray photoelectron spectroscopy (XPS) was used to evaluate surface composition and film uniformity, which was also verified by ellipsometry and optical reflectometry. Film thicknesses for the two preparation methods are compared, and the iridescence that arises in thicker spin-coated films is examined.

Experimental Details

Materials. Cationic poly(allylamine hydrochloride) (PAH) (M_w = 60 000 g/mol) was obtained from Polysciences (Warrington, PA) and used as received. Deionized water (18.2 MΩ·cm, Millipore Milli-Q purification system) was used without pH adjustments to prepare aqueous solutions with concentrations of 10^{-2} M PAH. Anionic cellulose nanocrystals were prepared by acid hydrolysis of cotton from Whatman cellulose filter aid (ashless powder, catalog no. 1700025), and a 1% solution, as measured by gravimetric analysis, was used unless otherwise noted. Error values are calculated at 95% confidence from replicate measurements.

Sulfuric Acid Hydrolysis of Cellulose. Suspensions of nanocrystalline cellulose were prepared as follows. Hydrolysis was carried out with 64% (w/w) sulfuric acid at 45°C for 45 min with constant stirring. Typically, 40 g of filter aid (dried at 105°C for 30 min) was treated with 700 mL of acid. Immediately following the acid hydrolysis, the suspension was diluted 10-fold with deionized water to quench the reaction. The suspension was centrifuged at 6000 rpm for 10 min to concentrate the cellulose and to remove excess aqueous acid. The resultant precipitate was rinsed, recentrifuged, and dialyzed against water for 5 days until constant neutral pH was achieved. Mixed-bed research-grade resin (Sigma) was added to the cellulose suspension for 48 h and then removed by filtering through hardened ashless filter paper (Whatman 541). The suspension was sonicated repeatedly (Vibracell Sonicator, Sonics and Materials Inc., Danbury, CT) at 60% output (with cooling in an ice bath) to create cellulose crystals of colloidal dimensions. The resultant aqueous suspension was approximately 1% cellulose by weight (experimental yield of 62%) and the concentration was increased by evaporation at ambient conditions. The nanocrystals were converted from the protonated sulfonate ester to the sodium salt by conductometric titration (Orion conductivity cell 018010, with cell constant K = 0.987 cm^{-1} attached to a Fisher Scientific Accumet pH meter 50) with 0.0020 M NaOH. The surface charge density of cellulose nanocrystals was calculated to be 0.48 ± 0.05 e/nm^2 as measured by conductometric titration, with average crystal dimensions (from AFM images) of 129 nm × 10 nm. A small amount of toluene (50 μL per 1 L of suspension) was added to the cellulose suspension to avoid bacterial growth.

Film Preparation. Polyelectrolyte multilayer films were assembled on polished silicon <100> wafers obtained from WaferNet, Inc. The silicon wafers were cut to the desired dimensions (ca. 1.5 × 4.5 cm) and cleaned in a concentrated chromium(III) oxide/sulfuric acid bath for 24 h, followed by continuous rinsing with purified water. The multilayer films were prepared immediately after substrate cleaning. Two film preparation techniques were used: solution-dipping and spin-coating. The dipping procedure included a 25-min immersion of the wafer in a 250 mL bath of 10^{-2} m PAH, followed by three consecutive 250 mL rinse baths of deionized water: the first rinse bath was 1.0 min in duration, and the second and third rinse baths were for 2.0 min each (for a total rinsing time of 5 min). The wafer was then exposed to a 1.0% cellulose nanocrystal suspension for 25 min, followed by

identical rinsing steps. This cyclic process was carried out by use of an automated dipper (Shandon Varistain 24−4, Thermo Electron Corp.) until the desired number of layers was deposited. The assembled films were dried with compressed air and stored at 21 °C under vacuum. Spin-coated films were made with a commercial spin coater (Spin Processor, Laurell Technologies). In this case, 0.5 mL of 10^{-2} M PAH was poured on a stationary wafer, which was then accelerated at 1260 rpm/s and spun at 3000 rpm for 40 s. The film was then rinsed with 1.0 mL of deionized water and spun at 3000 rpm for 40 s. This rinsing procedure was repeated three times. Cellulose nanocrystal suspension was filtered through a 0.8 μm filter unit (Millipore) directly onto the PAH layer, spun, and rinsed following the same protocol. One bilayer is defined as a single deposition step of PAH followed by rinsing and an adsorption step with cellulose with rinsing; thus integer bilayers have cellulose as the outermost layer and half-integer bilayers end with PAH. Multilayered films containing 1 bilayer, $(PAH/cellulose)_1$, up to 25 bilayers, $(PAH/cellulose)_{25}$, were assembled.

Optical Characterization. A Multiskop (Optrel, Germany) single-wavelength (633 nm) null-ellipsometer at a fixed angle of 70° off normal was used to measure the film thickness of SiO_2 as well as the first PAH layer on Si. Films containing cellulose nanocrystals were difficult to measure by ellipsometry due to the birefringent nature of the crystals. Three techniques were used in combination to determine the film thickness: scratch-height analysis by AFM, optical reflectometry (λ range of 200−1500 nm, fixed angle = 3° 20″ off normal), and ellipsometry. Near-normal reflectivity of the multilayers on Si was measured with the diffuse reflectance accessory (DRA 2500) using a Cary 5000 ultraviolet/visible/near-infrared spectrophotometer (Varian, Inc.). Theoretical reflectivity was calculated by the transfer matrix method implemented in Mathematica. The method, described in *Optics* by Hecht[47] and used in similar studies,[16] computes a characteristic matrix of the system that results from the product of individual matrices for each layer in the film.[48] The film model used here assumed four layers (three unique interfaces): (1) a Si substrate ($n = 3.8858 - i0.002$), (2) a SiO_2 18 Å thick layer ($n = 1.4598$), (3) the multilayer film [n(PAH) = 1.45, $n(\text{cellulose})_{\parallel} = 1.544$, $n(\text{cellulose})_{\perp} = 1.618$], and (4) air ($n = 1.000$). It was determined that, for films in this thickness range with the refractive indices used, the theoretical data were identical regardless of whether a multilayer "slab" [n(film) = 1.50, mean refractive index calculated from fitted reflectivity data] or structured multilayer "stack" geometry was assumed. The experimental reflectivity data was fitted to the model (by the least-squares fitting procedure) to determine the refractive indices of the multilayer films. Delta and Psi values were collected from the ellipsometer and thickness was calculated by use of the Multiskop software (Elli, version 5.2) with the fixed refractive indices determined from reflectometry.

Atomic Force Microscopy. Film surface morphology was imaged by use of a NanoScope IIIa atomic force microscope (Digital Instruments) with the J piezoelectric scanner. Images were collected in contact and tapping modes with NP SiN_3 tips (spring constant 0.06 N/m, Digital Instruments) and Ultrasharp Si tips (spring constant 5.7 N/m, resonant frequency ca. 160 kHz, NSC14 series, MikroMasch), respectively. The multilayer thickness was determined by scratch-height analysis on a 50 μm image by use of the section analysis tool provided with the AFM software (Digital Instruments, version 4.32r1). Root-mean-squared (RMS) roughness was determined by AFM image analysis on scan sizes of 2, 4, and 8 μm.

X-ray Photoelectron Spectroscopy. The XPS measurements were performed with an Axis Ultra electron spectrometer (Kratos Analytical) using a monochromated Al Kα X-ray source (12.5 kV, 8 mA). Multilayered films, $(PAH/cellulose)_1$ and $(PAH/cellulose)_2$, prepared by solution-dipping and spin-coating were cut into 1 cm^2 samples from the center of each film. For the analysis of these films, a flood gun was used to avoid charging of the surface. Analysis area was 2 mm^2 at a takeoff angle of 90° under ultrahigh vacuum conditions. The low-resolution survey scans were taken with a 1 eV step and 160 eV analyzer pass energy; high-resolution spectra were taken with a 0.1 eV step and 40 eV analyzer pass energy. The measurements were repeated several times on each sample.

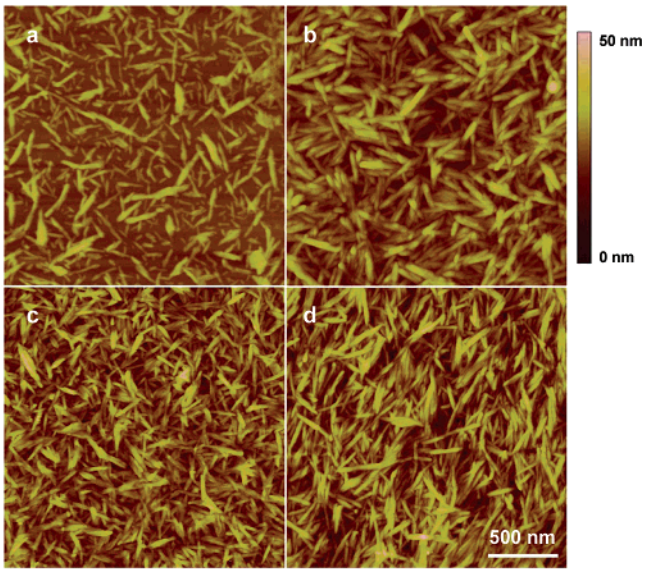

Figure 2. Tapping-mode AFM height images (2 μm × 2 μm) of the surface of $(PAH/cellulose)_{2.5}$ prepared by (a) solution-dipping and (b) spin-coating and the surface of $(PAH/cellulose)_{25}$ prepared by (c) solution-dipping and (d) spin-coating.

Scanning Electron Microscopy. Structure and morphologies of the thin films were examined by use of a Hitachi S-4700 cold field emission scanning electron microscope (FE-SEM). The samples were either carbon-coated or Au−Pd-coated prior to imaging.

Results and Discussion

Cellulose nanocrystals were successfully incorporated into polyelectrolyte multilayer films containing PAH. The two film preparation methods, solution-dipping and spin-coating, showed remarkable differences in film thickness but similar film surface morphology and roughness. Complete surface coverage of the silicon substrate occurred after 1 bilayer was deposited by spin-coating but required more than five adsorption steps (2.5 bilayers) for the solution-dipped films. Figure 2 shows AFM height images acquired in tapping mode for the two preparation methods. The crystals always adsorb along their long axis and smaller crystals adsorb faster than the longer crystals, in the case of solution-dipping. Panels a and b compare solution-dipped and spin-coated films of $(PAH/cellulose)_{2.5}$, a multilayer film containing 2 bilayers and a capping layer of PAH. Cellulose nanocrystals have dimensions of 5−10 nm by 100−200 nm; the length polydispersity of the nanocrystals is apparent and has been found previously[49] to be 1.2−1.3. The spin-coated film has a larger amount of material adsorbed, although in a few places the bare substrate can be seen. The thin films shown in Figure 2a,b have PAH as the outermost layer, whereas the thicker films shown in Figure 2c,d, $(PAH/cellulose)_{25}$, contain cellulose nanocrystals as the outermost layer. The surface morphology of the two different capping layers is indistinguishable; topological features indicative of aggregated polymer are not seen in AFM images of films containing 2.5−25 bilayers, prepared by both methods. In some cases, however, transfer of PAH to the AFM tip did result in tip-broadening artifacts.[50] Previous reports concur that, during the first few deposition steps in the solution-dipping procedure, the substrates is often not saturated and changes in adsorption morphology are observed.[25] No detectable difference between surface morphologies was seen in solution-dipped and spin-coated films.

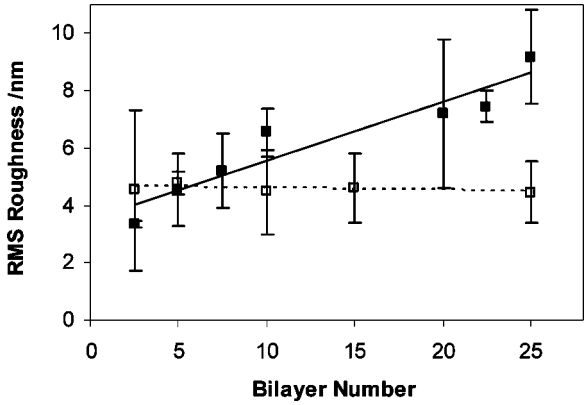

Figure 3. Root-mean-squared surface roughness as a function of PAH/cellulose bilayer number determined from contact-mode AFM height images on 8 μm^2, 4 μm^2, and 2 μm^2 scans over different areas of the sample. Films were prepared by solution-dipping (■) and spin-coating (□), and error bars are calculated at 95% confidence from replicate measurements.

The main criteria for the formation of polyelectrolye multilayer films are that the two components be oppositely and sufficiently charged. Polymer complexation, enthalpy release as ionic bonds form, and entropy increase, due to liberated counterions and the destruction of solvation shells around ionic groups when a polyelectrolyte binds to a surface, are believed to drive the adsorption process.[10,14] Film deposition occurred under neutral pH conditions to ensure that the weak polyelectrolyte PAH ($pK_a \sim 8.7$) was fully charged. Neutron reflectivity of poly(styrene sulfonate) (PSS)/PAH multilayers suggest polyelectrolyte mass densities of 0.81 and 1.13 g/cm^3 for the fully hydrated and dehydrated films, respectively.[51] These values indicate that the charge density for PAH with one charged group per repeat unit is 3.00−3.75 e/nm^2 depending on the amount of water in the film. The cellulose nanocrystals are negatively charged due to the addition of sulfate ester groups on the surface of the crystals during the hydrolysis process. The sulfur content in the cellulose suspension was measured by conductometric titration and determined to be 0.67 ± 0.05 wt %, which corresponds to a surface charge density of 0.48 ± 0.04 e/nm^2. The flexible polymer PAH is therefore 6−8 times more charged than the rigid cellulose nanocrystals, making charge compensation sterically impossible.

Figure 3 indicates that the films of PAH and cellulose nanocrystals are relatively smooth (RMS roughness below 10 nm). The films prepared by solution-dipping show a slight increase in roughness per deposition step, which follows a linear trend. This is expected since nanocrystals have no preference between adsorbing on top of each other and adsorbing in the bare spaces. Spin-coated PAH/cellulose films are more uniform in roughness with a negligible change upon the addition of more layers. The spin-coated films are smoother than the solution-dipped films, consistent with other reports,[52] due to both increased surface coverage and the downward force exerted on the substrate during the rapid expulsion of fluid in the spin-coating process.

Some orientation of the cellulose nanocrystals is visible in the spin-coated films as more layers are deposited (Figure 2d). This nanoscale order occurs to different extents in various regions of the film. The alignment is radial and arises from viscous shear as the suspension of cellulose nanocrystals flows outward during spin-coating. Due to the birefringence of the cellulose nanocrystals, this radial order can be seen by observing the film between crossed polarizers (Figure 4). The 1 cm^2 area (Figure 4a), shows $(PAH/cellulose)_{10}$ spin-coated onto a glass

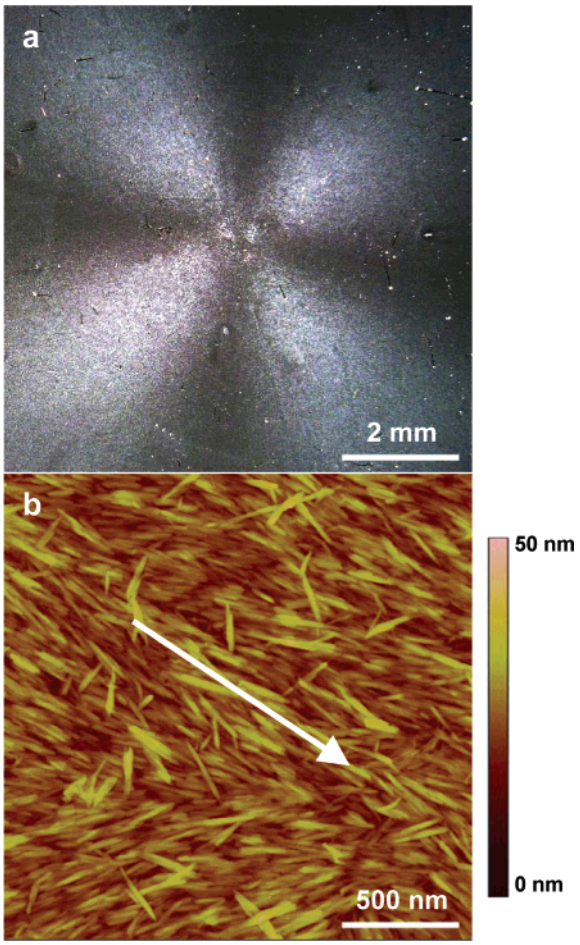

Figure 4. Orientation of cellulose nanocrystals, seen on many length scales. (a) Polarized-light microscopic image of $(PAH/cellulose)_{10}$ prepared by spin-coating on a glass substrate. The radial orientation and anisotropy of the crystals results in a Maltese cross pattern, visible between crossed polarizers. (b) Tapping-mode AFM height image (2 $\mu m \times 2$ μm) of a $(PAH/cellulose)_{15}$ film prepared by spin-coating on Si. One region of the pattern shown in (a) displays alignment of the nanocrystals in the direction of the arrow. Some areas of the multilayered films show more orientation than others.

substrate. The underside of the glass slide was cleaned but dust and scratches can be seen in the image nonetheless. The alignment contains many defects and it is noteworthy that the deposition of a single layer of cellulose nanocrystals on PAH does not show nearly as much orientation as is seen in the thicker films. Nonetheless, alignment of cellulose nanocrystals in nanocomposites has previously been shown to increase mechanical strength,[34] and nanocrystal orientation is therefore a promising feature of films prepared by spin-coating. As with all nanocomposites, the reinforcing agent and adhesive binding matrix must interact favorably; this is the case for this system. However, alignment defects and spatial inhomogeneities will diminish the strengthening effects of the cellulose nanocrystals. Contrary to other nanomaterial preparation techniques, the LbL method is robust and relatively insensitive to defects, which are quickly hidden by adding further layers. As well, by adjusting the cellulose source and hydrolysis conditions, the aspect ratio and polydispersity can be adjusted for optimal reinforcing properties. Aligning the cellulose nanocrystals in LbL films by applying a high magnetic field has been attempted.[53]

Films prepared by both solution-dipping and spin-coating were found to be unaffected after 5 days immersion in water at

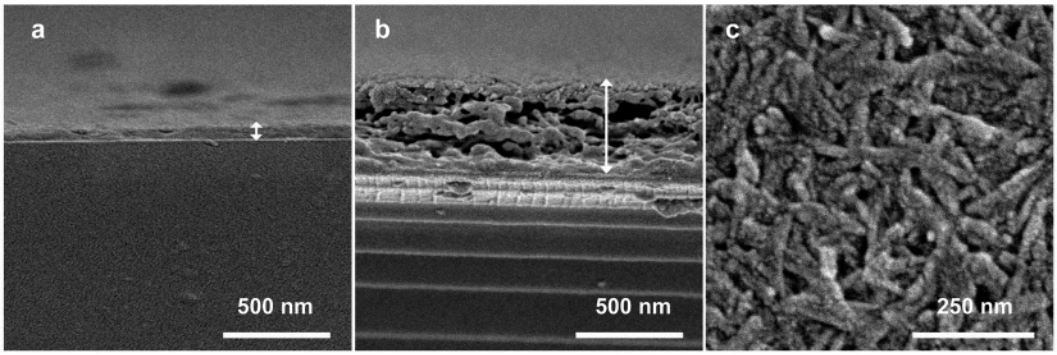

Figure 5. Scanning electron microscopic images of multilayered films of PAH and cellulose: (a) film edge of $(PAH/cellulose)_{25}$ prepared by solution-dipping, (b) film edge of $(PAH/cellulose)_{25}$ prepared by spin-coating (the horizontal white lines below the film are substrate fracture artifacts), and (c) surface topography of $(PAH/cellulose)_{25}$ prepared by solution-dipping. White arrows indicate the multilayer film thickness.

temperatures ranging from 10 to 100 °C. These results are consistent with previous reports on multilayer stability.[54] AFM images of the surface before and after exposure to water did not indicate any changes in the surface morphology. The alignment of nanocrystals that is seen for the thicker spin-coated films is retained when the films are placed in water. Ionic cross-linking between the two polyelectrolytes and interpenetration of PAH chains are the most probable cause for this stability. Conversely, thin films of pure nanocrystalline cellulose, prepared by spin-coating or solvent casting, swelled and then redispersed when exposed to water.[4] Annealing pure cellulose films under mild thermal conditions was found to increase the film stability, and we believe that heat-treating the polyelectrolyte multilayer films has a similar effect.

The spin-coating process has been used to make polyelectrolyte multilayers in previous reports.[18,27,46,52,55] For the case of linear polymers, spin-coating and solution-dipping methods are reported to give films of similar thickness.[24,45] It is assumed that these thicknesses are comparable because in both cases nonelectrostatically bound material is removed during the rinsing steps. Here, however, we have observed that the "kinetically driven" assembly process of spin-coating has incorporated substantially more material into the film than is adsorbed during solution-dipping. The difference in film thickness between solution-dipped and spin-coated films is considerable and is shown in the SEM side-view images of $(PAH/cellulose)_{25}$ (Figure 5, panels a and b, respectively). While film thickness does increases with bilayer number, the growth of spin-coated films is much faster. The difference in film thickness becomes more pronounced as the number of bilayers increases. For $(PAH/cellulose)_{25}$, the films prepared by solution-dipping and spin-coating are 71 ± 3 nm and 499 ± 14 nm, respectively (as measured from the SEM images). This corresponds to a spin-coated film that is 7 times thicker than the film prepared by solution-dipping. While an exhaustive study of spin-coated film thickness as a function of solution concentration, volume, and spin speed has not been conducted, use of identical dipping and spinning solution concentrations leads to films of significantly different thicknesses. This has not been reported previously.

Another indication that the spin-coated films were much thicker than the solution-dipped films was the strong interference colors, visible for all spin-coated films of more than 10 bilayers. Solution-dipped films were transparent with minimal cloudiness, except near the film edges where droplet accumulation creates a thicker coating. UV/Vis spectroscopy is one of the easiest ways to monitor multilayer growth[14] and could be used here only to measure the build-up of the solution-dipped films. For the intensely colored spin-coated films, thin film interference peaks (Fabry−Perot fringes) were monitored by optical reflectometry (Figure 6). The reflectivity spectra and their corresponding film colors are shown in Figure 6 for PAH/cellulose multilayer films made by spin-coating. These colors are due to destructive interference between light reflected from the air−film interface and from the film−substrate interface. The reflected light intensity is a function of the number of layers and the mean refractive index of the film. Scattering was determined to be minimal because the size of the films was much smaller than the wavelength at which they were probed. As expected,[40] the number of fringes increased with the number of deposition steps, that is, film thickness.

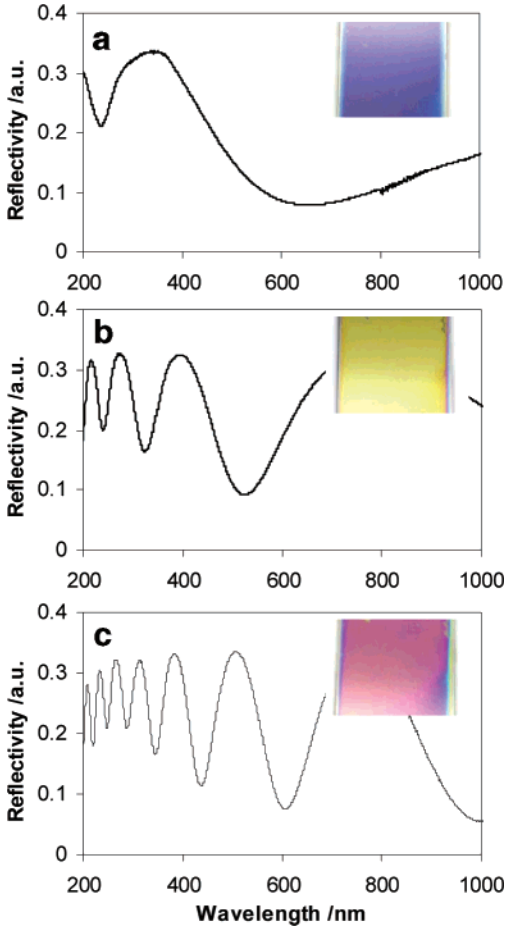

Figure 6. Wavelength-dependent reflectivity (thin film interference patterns) of multilayered films of PAH/cellulose prepared by spin-coating on Si: (a) film of $(PAH/cellulose)_{10}$, (b) film of $(PAH/cellulose)_{15}$, and (c) film of $(PAH/cellulose)_{25}$. Insets are digital photographs of 1 cm × 1 cm pieces of the respective films.

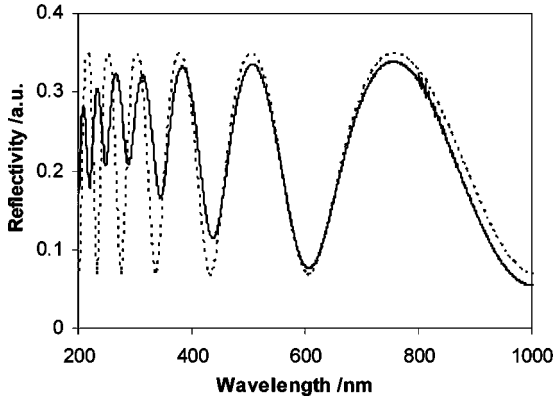

Figure 7. Comparison of experimental reflectivity data (solid line) with theoretical (transfer-matrix method) reflectivity data (dotted line) for $(PAH/cellulose)_{25}$ prepared by spin-coating. The film thickness was measured to be 499 ± 14 nm from SEM, and the mean refractive index was 1.50 ± 0.01, determined from reflectometry.

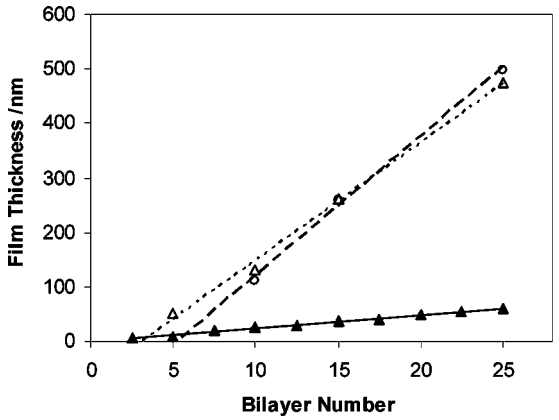

Figure 8. Variation in film thickness of PAH/cellulose films with bilayer number measured by ellipsometry (triangles) and reflectivity (circles) for solution-dipped films (solid symbols) and spin-coated films (open symbols). The multilayer films prepared by spin-coating are much thicker. Lines are linear least-squares fits of the data.

To determine the film thickness, three methods were employed. Initial ellipsometry measurements on multilayered films gave either physically unreasonable thicknesses or indicated that the films were thinner than expected from AFM scratch-height analysis. This was assumed to be due to both intrinsic and form birefringence of the crystals. Using the reflectivity data, we were able to calculate the mean refractive index of the films and set it constant during the ellipsometry measurements. Reflectivity was modeled by the transfer matrix method[47] and the mean refractive index was determined to be 1.50 ± 0.01 for films prepared by both methods. Figure 7 shows the agreement between experimental and theoretical reflectivity data for $(PAH/cellulose)_{25}$ prepared by spin-coating. Discrepancies in the 200−300 nm wavelength range are due to the changes in the refractive index with wavelength of Si and SiO_2, which were not accounted for in the model.

Once the mean refractive index was known, film thickness was determined by ellipsometry; the results are shown in Figure 8. For the colored spin-coated films, we found that the thickness results from ellipsometry and reflectometry are in accord. Multilayer buildup is linear, with an average thickness increase per bilayer of 2 nm and 16 nm (~2 cellulose nanocrystals thick) for films prepared by solution-dipping and spin-coating, respectively. This would indicate that 3−5 solution adsorption steps of cellulose nanocrystals are required to form a complete surface covering "layer". AFM scratch-height analysis was a reliable method for measuring film thickness only below 50 nm. Although the *z*-range of the AFM is much larger than 50 nm, scan size and scan rate substantially affect the instrument's measurement of large peaks and valleys. Additionally, use of an AFM with an open feedback loop makes quantitative analysis problematic. The approximately linear growth of multilayers prepared by both methods is standard for the LbL assembly[56] and is often a sign of well-ordered films.[27]

Spin-coating sequential cellulose nanocrystals (without rinsing or alternating with polycation layers) makes films that exhibit similar colors.[50] The color is less uniform around the edges than when cellulose nanocrystals are spun onto a precursor layer of PAH. The incorporation of PAH layers is therefore believed to aid in the formation of stable uniform colored films.

As discussed above, the multilayer films prepared by the solution-dipping adsorption process contain significantly less material than the spin-coated multilayers. This suggests that the dipping process for cellulose nanocrystals is diffusion- (or transport-) limited. Because PAH is much more charged than cellulose, adsorption of more than one layer of cellulose nanocrystals is expected if charge compensation is to be achieved. The deposition time chosen for multilayering was 25 min, although experimental results for linear polymers (PAH, poly(acrylic acid), polystyrene sulfonate (PSS), and poly-{1-[5-(3-carboxy-4-hydroxyphenylazo)benzenesulfonamino]-1,2-ethanediyl, sodium salt}) have shown that adsorption saturates before 60 s.[57] Empirically chosen adsorption times in LbL assembly are 10−20 min to allow for a two-step adsorption process consisting of a fast initial adsorption of only a few segments, followed by a rearrangement, relaxation, and packing step.[10,45] The apparent diffusion coefficient of cellulose nanocrystals with Na^+ counterions has been measured[58] by dynamic light scattering and was reported as 4.7×10^{-8} cm^2/s. The mean time to capture sufficient crystals for full surface coverage (based on random walk statistics in one dimension[59]) is 90 min for a 1% cellulose nanocrystal suspension in a 250 mL beaker. This approximate calculation also indicates that a 10% solution would require only 9 min for complete surface coverage and emphasizes the adsorption dependence on cellulose suspension concentration and adsorption time. In the spin-coating process the solvent evaporates quickly, resulting in a more concentrated suspension and hence, presumably, a thicker layer.

The SEM cross-sections of the films (Figure 5) show significant disorder. An extensive amount of interpenetration generally occurs within polyelectrolyte multilayers, and the high degree of order sometimes observed for films containing uniform spherical colloidal particles[52] is not expected for the polydisperse cellulose nanocrystals. Films prepared by spin-coating appear to be more porous than solution-dipped films when investigated by SEM (Figure 5). Reflectometry and ellipsometry, however, indicate that the refractive indices are within error at 1.50 ± 0.01. Evidently, the mean refractive index of the films is dominated by the topological packing of the cellulose nanocrystals, with little influence from PAH. Most probably, the porelike spaces seen in Figure 5a are a result of the freeze−fracturing method used to prepare samples for SEM; nanocrystals in the less dense region of the film are more easily detached when the film is broken.

The zone model for flexible polyelectrolyte multilayer films[14,55] includes three distinct regions: zone I is close to and strongly influenced by the substrate, zone II is the neutral bulk region, and zone III is the area closest to the film−air (or film−solution) interface. Zones I and III are charged and contain varying amounts of counterions because they are normally

unable to complex in 1:1 stoichiometric proportions. As film growth occurs, zones I and III stay constant in thickness as zone II expands.[10] In contrast, here, the large rigid cellulose nanocrystals with low charge density are never able to complex stoichiometrically but SEM data are consistent with the idea that three distinct regions exist. On the basis of the large excess of positive charge, a substantial number of Cl^- counterions are expected to remain in the films. In this case, it appears that the films are able to pack tighter at the interfaces while displaying substantial porosity in the middle region. Other support for varied architecture in LbL assembled films include a recent neutron reflectivity study of polyelectrolyte multilayers indicating a similar three-region model: dense polymer near the substrate, interpenetrated bulk middle region and a diffuse free surface.[60] Additionally, in weak polyelectrolyte systems, pK_as for adsorbed polymers are known to differ from solution pK_as, and a shift in the charge density would likely affect the packing of polymer throughout the film.[43]

In previous work by Podsiadlo et al.,[42] LbL films were prepared from cellulose nanocrystals functionalized with sulfonate ester groups in the acid form (whereas we use the sodium salt form), and they used a strong polyelectrolyte, poly(diallyldimethylammonium chloride) (PDDA), as the polycation. Films were assembled by a similar solution-dipping protocol; however, rinse baths were adjusted to pH 2−3 to be consistent with the acidic cellulose nanocrystal suspension pH. The average thickness increment is reported as 11 nm/bilayer, which is significantly larger than what we have observed for our solution-dipped films. This value is closer to the thicknesses obtained for spin-coated films, which were not diffusion-limited. The study by Podsiadlo et al. does not report dipping solution concentrations, making a direct comparison difficult; it is, however, possible that they were solution-dipping at concentrations where adsorption was not diffusion-limited. Surface morphologies of films prepared by Podsiadlo et al. are very similar to ours with more visible aggregation of cellulose nanocrystals; this may be a result of the acidic LbL dipping conditions, the polycation PDDA, or incomplete degradation/separation of the nanocrystals during suspension preparation. We can conclude from these studies that the LbL technique applied to cellulose nanocrystals and various polycations is robust and sufficient to create densely packed uniform films with a choice of tunable properties.

Optical Properties. Films prepared by spin-coating were substantially thicker than solution-dipped films and displayed angle-dependent colors. The characterization of multilayer optical properties is challenging due to the anisotropic nature of cellulose; therefore, the incident angles used in optical reflectometry were chosen to minimize this aspect. Comparing reflectometry results for diffuse and specular reflectance indicates that reflectivity is more than 99% specular. The maximum reflectivity measured for a clean Si wafer is 0.4 for both S and P polarized light at incident angles near normal. The PAH/cellulose film decreased the reflectivity properties of the wafer by ca. 10% while maintaining the "mirrorlike" specular reflectance. It should be apparent that although suspensions of cellulose nanocrystals are known for their chiral nematic liquid crystalline properties[61−64] and can be solvent-cast into irridescent films,[4,65] the angle-dependent colors seen in these PAH/cellulose films were not a result of chiral nematic structural order. The fingerprint texture, characteristic of chiral nematic liquid crystal phases, was not observed by polarization microscopy; the ordering of a lyotropic liquid crystal system, like cellulose nanocrystal suspensions, can be achieved only above a critical concentration.

Table 1. XPS Results

	total C (%)	total Si (%)	O/C ratio	$C_{cellulose}/C_{PAH}$ ratio
solution-dipped, 1 bilayer	10	38	3.5	1.2
solution-dipped, 2 bilayers	19	32	1.7	3.1
spin-coated, 1 bilayer	45	10	0.85	0.39
spin-coated, 2 bilayers	56	1	0.73	0.33

It is also interesting to note that iridescent films can be made when only one of the multilayer film components is spin-coated. Films of 10−25 bilayers were prepared whereby PAH was solution-dipped and cellulose was spin-coated (PAH_{dip}/$cellulose_{spin}$) and vice versa. When the cellulose nanocrystals were the spin-coated component, the film growth was faster than for films with spin-coated PAH but slower than when both polyelectrolytes were spin-coated. For example: the film (PAH_{dip}/$cellulose_{spin}$)$_{25}$ is 2 times thicker than (PAH_{spin}/$cellulose_{dip}$)$_{25}$ and similar in thickness to (PAH_{spin}/$cellulose_{spin}$)$_{15}$. These films are also stable when exposed to water, and while it was expected that films with spin-coated cellulose nanocrystals would exhibit similar optical properties, we were surprised to see the fast film growth for (PAH_{spin}/$cellulose_{dip}$). Films of (PAH_{spin}/$cellulose_{dip}$) were thicker than (PAH_{dip}/$cellulose_{dip}$) films, and this is most likely due to the interpenetration of the "extra" polymer chains that go down during spin-coating. Clearly, in this case, spin-coating leads to thicker layers at each deposition step, mainly due to enhanced concentration at the substrate surface.

XPS Analysis. Films composed of 1 or 2 bilayers of PAH and cellulose nanocrystals, prepared by both solution-dipping and spin-coating, were analyzed by XPS. In a quantitative XPS study, the top 20 nm are analyzed, although the signal decays exponentially with depth and is therefore biased toward the top composition of the film.[66] Absolute measurements are difficult, and normally the imprecision is taken to be ±10%. For pure cellulose, $(C_6O_5H_9)_n$, the theoretical ratio of oxygen to carbon is 0.83. The carbon 1s peaks can be deconvoluted into C1 (carbon bound to H), C2 (carbon bound to O), and C3 (O−C−O or C═O) with increasing binding energies, respectively.[67] Cellulose does not contain any carbon atoms bound to hydrogen, yet XPS analysis of model cellulose surfaces normally contains a small amount of hydrocarbon surface contaminant. In addition to oxygen and carbon, peaks were expected from the nitrogen and chlorine in the PAH. A large Si peak was also seen from the substrate because the LbL assembled films analyzed had thicknesses below 20 nm. Trace amounts of sulfur were observed from sulfate ester groups on the cellulose nanocrystals as well as from the sulfuric acid used to clean the Si wafers. Phosphorus and aluminum peaks were detected and are assumed to be doping impurities in Si. Due to the thin nature of the multilayer films (and the large Si peak), it is believed that we are nearing the limits of this technique.

The XPS signal from Si decreases as the total C signal increases and is essentially zero when the multilayer thickness exceeds the XPS escape depth. The O/C ratio and the (C2 + C3)/C1 ratio (i.e., $C_{cellulose}/C_{PAH}$) are reported in Table 1 for the four samples (atomic percentages indicated are equivalent to mole percentages[66]). Because the solution-dipped films are much thinner, the C % is low, the Si % is high, and the oxygen in SiO_2 makes the O/C ratio large. It is impossible to deconvolute oxygen in the oxide layer from oxygen in cellulose. From the XPS data we can conclude that adding bilayers increases the amount of material in the film and that spin-coated films

have more polymeric material (relative to cellulose nanocrystals) adsorbed than solution-dipped films. XPS data from 2 bilayers of spin-coated polymer are the most representative because the low silicon (and therefore SiO_2) signals exert the least influence on the component ratios. An O/C ratio of less than 0.83 is expected from the presence of PAH carbon and in accordance, was found to be 0.73. The low $C_{Cellulose}/C_{PAH}$ ratios for the spin-coated films agree with the reasoning that the amount of material deposited during spin-coating is inversely proportional to the logarithm of polymer molecular weight.[46] XPS thus suggests that the spin-coated films contain about 3 times more PAH than nanocrystalline cellulose.

Many reports have shown that multilayering without electrostatics is possible if H-bonding, $\pi-\pi$ stacking forces, hydrophobic interactions, charge-transfer interactions, covalent bonding, or specific interactions are operative.[10,14] We also attempted solution-dipping with poly(ethylene oxide) (PEO) but this did not result in film buildup because PEO is not charged and H-bonding between PEO and cellulose was not sufficient. Our system is therefore unlike those where entanglement and interpenetration of layers is sufficient to deposit sequential polyelectrolyte layers with like charges.[44] Here, the discrepancies with cited literature are most likely due to the large size of the cellulose nanocrystals and their requirement for strong interactions to anchor them to the surface. The fact that film formation was not observed for PEO and cellulose justifies that multilayer film growth in the PAH/cellulose system is due to electrostatics and not purely due to physisorption or specific interactions of cellulose nanocrystals.

Films prepared by solution-dipping are normally not transferable from their substrates because they lack mechanical stability.[18] In our system, spin-coating can be used to achieve the film thicknesses required for free-standing films. Dimensions of the cellulose nanocrystals ensure smooth films and a wide thickness range when compared to the majority of studies, which use colloidal particles larger than 0.5 μm.[20,26,40] Most notably, spin-coating allows for the iridescent colors to be fine-tuned in a minimal number of steps when contrasted with linear polymer systems requiring over 1000 deposition steps to achieve similar optical properties.[23]

Conclusion

Thin multilayered films incorporating polyelectrolyte layers and nanocrystalline cellulose layers were prepared by the electrostatic layer-by-layer methodology, as well as by a spin-coating variant. Both techniques gave rise to smooth and stable thin films, as confirmed by AFM surface morphology measurements as well as SEM investigations. Thus both techniques are viable for producing structured nanocomposites, where the large aspect ratio cellulose units may serve to strengthen the elastic polymer matrix.

Noteworthy differences were found between the two film preparation strategies. In particular, the films prepared by spin-coating were substantially thicker than corresponding solution-dipped films. Furthermore, the anisotropic cellulose nanocrystals were found to be ordered by the radial centrifugal forces inherent to spin-coating. The ability to orient the cellulose crystals is also useful for creating nanocomposites with desired, possibly anisotropic mechanical properties. The films prepared with these techniques have good optical properties, displaying thin-film interference colors, as characterized by optical reflectometry. The film preparation techniques we have presented allow the creation of structurally controlled thin films with tunable mechanical and optical properties. In addition to obvious applications as coatings and biocompatible materials, this system may also provide an improved understanding of basic cellulose surface interactions.

Acknowledgment. We thank NSERC Canada and Paprican for financial support, Professors C. J. Barrett and R. B. Lennox for generous use of laboratory equipment, A. Lejeune (UQTR) for XPS data acquisition, and L. Mongeon (McGill) for help with SEM. Useful discussions with K. Yager, O. Tanchak, and Professors T. van de Ven and R. H. Marchessault are acknowledged.

References and Notes

(1) Battista, O. A.; Coppick, S.; Howsmon, J. A.; Morehead, F. F.; Sisson, W. A. *J. Ind. Eng. Chem. (Washington, D. C.)* **1956**, *48*, 333−335.
(2) Ranby, B. G. *Discuss. Faraday Soc.* **1951** (No. 11), 158−164, discussion 208−113.
(3) Mathew, A. P.; Oksman, K.; Sain, M. *J. Appl. Polym. Sci.* **2005**, *97*, 2014−2025.
(4) Edgar, C. D.; Gray, D. G. *Cellulose (Dordrecht, Neth.)* **2003**, *10*, 299−306.
(5) Kontturi, E.; Thune, P. C.; Niemantsverdriet, J. W. H. *Langmuir* **2003**, *19*, 5735−5741.
(6) Notley, S. M.; Wagberg, L. *Biomacromolecules* **2005**, *6*, 1586−1591.
(7) Gunnars, S.; Wagberg, L.; Cohen Stuart, M. A. *Cellulose (Dordrecht, Neth.)* **2002**, *9*, 239−249.
(8) Carambassis, A.; Rutland, M. W. *Langmuir* **1999**, *15*, 5584−5590.
(9) Notley, S. M.; Pettersson, B.; Waagberg, L. *J. Am. Chem. Soc.* **2004**, *126*, 13930−13931.
(10) Bertrand, P.; Jonas, A.; Laschewsky, A.; Legras, R. *Macromol. Rapid Commun.* **2000**, *21*, 319−348.
(11) Torn, L. H.; Koopal, L. K.; de Keizer, A.; Lyklema, J. *Langmuir* **2005**, *21*, 7768−7775.
(12) Dong, X. M.; Revol, J. F.; Gray, D. G. *Cellulose (Dordrecht, Neth.)* **1998**, *5*, 19−32.
(13) Decher, G. *Science (Washington, D. C.)* **1997**, *277*, 1232−1237.
(14) Decher, G.; Schlenoff, J. B. *Multilayer Thin Films*; Wiley−VCH: New York, 2002.
(15) Hiller, J. A.; Mendelsohn, J. D.; Rubner, M. F. *Nat. Mater.* **2002**, *1*, 59−63.
(16) Nolte, A. J.; Rubner, M. F.; Cohen, R. E. *Langmuir* **2004**, *20*, 3304−3310.
(17) Cong, H.; Cao, W. *Langmuir* **2004**, *20*, 8049−8053.
(18) Jiang, C.; Markutsa, S.; Pikus, Y.; Tsukruk, V. V. *Nat. Mater.* **2004**, *3*, 721−728.
(19) Lehr, B.; Seufert, M.; Wenz, G.; Decher, G. *Supramol. Sci.* **1996**, *2*, 199−207.
(20) Masse, P.; Ravaine, S. *Chem. Mater* **2005**, *17*, 4244−4249.
(21) Tang, Z.; Kotov, N. A.; Magonov, S.; Ozturk, B. *Nat. Mater.* **2003**, *2*, 413−418.
(22) Strharsky, R.; Wheatley, J. *Opt. Photonics News* **2002**, *13*, 35−40.
(23) Zhai, L.; Nolte, A. J.; Cohen, R. E.; Rubner, M. F. *Macromolecules* **2004**, *37*, 6113−6123.
(24) Burke, S.; Barrett, C. J. *Biomacromolecules* **2003**, *4*, 1773−1783.
(25) Fujita, S.; Shiratori, S. *Nanotechnology* **2005**, *16*, 1821−1827.
(26) Soo Ahn, J.; Hammond, P. T.; Rubner, M. F.; Lee, I. *Colloids Surf., A* **2005**, *259*, 45−53.
(27) Jiang, C.; Markutsa, S.; Tsukruk, V. V. *Adv. Mater. (Weinheim, Ger.)* **2004**, *16*, 157−161.
(28) Muller, M.; Brissova, M.; Rieser, T.; Powers, A. C.; Lunkwitz, K. *Mater. Sci. Eng., C* **1999**, *C8−C9*, 163−169.
(29) Feldheim, D. L.; Grabar, K. C.; Natan, M. J.; Mallouk, T. E. *J. Am. Chem. Soc.* **1996**, *118*, 7640−7641.
(30) Fang, M.; Ai, H.; Cush, R.; Russo, P.; Lvov, Y. *Abstracts of Papers*; 223rd ACS National Meeting, Orlando, FL, April 7−11, 2002; COLL-175.
(31) Cooper, T. M.; Campbell, A. L.; Crane, R. L. *Langmuir* **1995**, *11*, 2713−2718.
(32) de Souza Lima, M.; Borsali, R. *Macromol. Rapid Commun.* **2004**, *25*, 771−787.
(33) Beck-Candanedo, S.; Roman, M.; Gray, D. G. *Biomacromolecules* **2005**, *6*, 1048−1054.
(34) Orts, W.; Shey, J.; Imam, S.; Glenn, G.; Guttman, M.; Revol, J. F. *J. Polym. Environ.* **2005**, *13*, 301−306.
(35) Azizi Samir, M. A. S.; Alloin, F.; Sanchez, J.-Y.; Dufresne, A. *Polymer* **2004**, *45*, 4149−4157.

(36) Chauve, G.; Heux, L.; Arouini, R.; Mazeau, K. *Biomacromolecules* **2005**, *6*, 2025−2031.
(37) Chazeau, L.; Cavaille, J. Y.; Perez, J. *J. Polym. Sci., Part B: Polym. Phys.* **2000**, *38*, 383−392.
(38) Ljungberg, N.; Bonini, C.; Bortolussi, F.; Boisson, C.; Heux, L.; Cavaille, J. Y. *Biomacromolecules* **2005**, *6*, 2732−2739.
(39) Samir, M. A. S. A.; Alloin, F.; Dufresne, A. *Biomacromolecules* **2005**, *6*, 612−626.
(40) Reculusa, S.; Ravaine, S. *Chem. Mater* **2003**, *15*, 598−605.
(41) Cranston, E. D.; Gray, D. G.; Barrett, C. J. *Abstracts*; 32nd Northeast Regional Meeting of the American Chemical Society, Rochester, NY, October 31−November 3, 2004; GEN-332.
(42) Podsiadlo, P.; Choi, S.-Y.; Shim, B.; Lee, J.; Cuddihy, M.; Kotov, N. A. *Biomacromolecules* **2005**, *6*, 2914−2918.
(43) Burke, S.; Barrett, C. J. *Langmuir* **2003**, *19*, 3297−3303.
(44) Johal, M. S.; Casson, J. L.; Chiarelli, P. A.; Liu, D.-G.; Shaw, J. A.; Robinson, J. M.; Wang, H.-L. *Langmuir* **2003**, *19*, 8876−8881.
(45) Lee, S.-S.; Hong, J.-D.; Kim, C. H.; Kim, K.; Koo, J. P.; Lee, K.-B. *Macromolecules* **2001**, *34*, 5358−5360.
(46) Lee, S.-S.; Lee, K.-B.; Hong, J.-D. *Langmuir* **2003**, *19*, 7592−7596.
(47) Hecht, E. *Optics*, 4th ed.; Pearson Addison-Wesley: Reading, MA, 2001.
(48) Born, M.; Wolf, E. *Principles of Optics*; Pergamon: New York, 1964.
(49) Marchessault, R. H.; Morehead, F. F.; Koch, M. J. *J. Colloid Sci.* **1961**, *16*, 327−344.
(50) Lefebvre, J.; Gray, D. G. *Cellulose (Dordrecht, Neth.)* **2005**, *12*, 127−134.
(51) Loesche, M.; Schmitt, J.; Decher, G.; Bouwman, W. G.; Kjaer, K. *Macromolecules* **1998**, *31*, 8893−8906.
(52) Cho, J.; Char, K.; Hong, J.-D.; Lee, K.-B. *Adv. Mater. (Weinheim, Ger.)* **2001**, *13*, 1076−1078.
(53) Cranston, E. D.; Gray, D. G. *Sci. Technol. Adv. Mater.* **2006**, ***7***, 319−321.
(54) Mermut, O.; Barrett, C. J. *Analyst (Cambridge, U.K.)* **2001**, *126*, 1861−1865.
(55) Ladam, G.; Schaad, P.; Voegel, J. C.; Schaaf, P.; Decher, G.; Cuisinier, F. *Langmuir* **2000**, *16*, 1249−1255.
(56) Arys, X.; Fischer, P.; Jonas, A. M.; Koetse, M. M.; Laschewsky, A.; Legras, R.; Wischerhoff, E. *J. Am. Chem. Soc.* **2003**, *125*, 1859−1865.
(57) Mermut, O.; Barrett, C. J. *J. Phys. Chem. B* **2003**, *107*, 2525−2530.
(58) Dong, X. M.; Gray, D. G. *Langmuir* **1997**, *13*, 2404−2409.
(59) Berg, H. C. *Random walks in biology*; Princeton University Press: Princeton, NJ, 1993.
(60) Tanchak, O. M.; Yager, K. G.; Fritzsche, H.; Harroun, T.; Katsaras, J.; Barrett, C. J. *Langmuir* **2006**, *22*, 5137−5143.
(61) Revol, J. F.; Godbout, L.; Dong, X. M.; Gray, D. G.; Chanzy, H.; Maret, G. *Liq. Cryst.* **1994**, *16*, 127−134.
(62) Dong, X. M.; Kimura, T.; Revol, J.-F.; Gray, D. G. *Langmuir* **1996**, *12*, 2076−2082.
(63) Dong, X. M.; Gray, D. G. *Langmuir* **1997**, *13*, 3029−3034.
(64) Edgar, C. D.; Gray, D. G. *Macromolecules* **2002**, *35*, 7400−7406.
(65) Revol, J. F.; Godbout, L.; Gray, D. G. *J. Pulp Pap. Sci.* **1998**, *24*, 146−149.
(66) Istone, W. K. In *X-ray Photoelectron Spectroscopy in Surface Analysis of Paper*; Connors, T. E., Banerjee, Eds.; CRC Press: Boca Raton, FL, 1995, pp 235−268.
(67) Dorris, G. M.; Gray, D. G. *Cellul. Chem. Technol.* **1978**, *12*, 9−23.

BM0602886